SCIENTIFIC REPORTS

OPEN

Simulation of head and neck cancer oxygenation and doubling time in a 4D cellular model with angiogenesis

Jake C. Forster [ID]1,2, Michael J. J. Douglass1,2, Wendy M. Harriss-Phillips1,2 & Eva Bezak1,3

Tumor oxygenation has been correlated with treatment outcome for radiotherapy. In this work, the dependence of tumor oxygenation on tumor vascularity and blood oxygenation was determined quantitatively in a 4D stochastic computational model of head and neck squamous cell carcinoma (HNSCC) tumor growth and angiogenesis. Additionally, the impacts of the tumor oxygenation and the cancer stem cell (CSC) symmetric division probability on the tumor volume doubling time and the proportion of CSCs in the tumor were also quantified. Clinically relevant vascularities and blood oxygenations for HNSCC yielded tumor oxygenations in agreement with clinical data for HNSCC. The doubling time varied by a factor of 3 from well oxygenated tumors to the most severely hypoxic tumors of HNSCC. To obtain the doubling times and CSC proportions clinically observed in HNSCC, the model predicts a CSC symmetric division probability of approximately 2% before treatment. To obtain the doubling times clinically observed during treatment when accelerated repopulation is occurring, the model predicts a CSC symmetric division probability of approximately 50%, which also results in CSC proportions of 30–35% during this time.

While tumors are typically more vascularized than normal tissue, hypoxia will still arise in many tumors due to heterogeneity in the vascularity and depleted levels of blood oxygenation that occur when blood moves sluggishly through constricted and malformed vessels[1, 2]. Radiotherapy is a primary treatment modality for head and neck squamous cell carcinoma (HNSCC) and tumor oxygenation has been correlated with treatment outcome[3–5]. Another key factor influencing the treatment outcome is the rate of tumor regrowth during treatment. Radiotherapy is typically delivered over several weeks (an example of a conventional fractionation schedule for the treatment of HNSCC with X-rays is 2 Gy fractions, 5 days/week over 6 weeks), and after a certain time (the "kick-off time") the tumor initiates accelerated repopulation[6–8]. One of the key mechanisms responsible for accelerated repopulation is reportedly an increase in the symmetric division of cancer stem cells (CSCs). CSCs make up only a small proportion of the tumor cells[9], but each has the potential to regenerate the tumor and must be inactivated to achieve 100% local tumor control probability.

In previous work, a computational model was developed that simulates HNSCC tumor growth[10]. This is a 4D cellular model that includes the simulation of tumor angiogenesis. In the first part of the current work, this model was used to quantitatively map tumor properties, such as vascularity and blood oxygenation, to tumor oxygenation descriptors, such as the proportion of hypoxic cells, the mean cellular pO_2 and the necrotic volume. By constraining the vascularity and blood oxygenation to values that have been clinically observed in HNSCC, values of tumor oxygenation descriptors were obtained for HNSCC and compared with clinical data.

In the second part of the work presented here, the effect of tumor oxygenation on the tumor volume doubling time for HNSCC was quantitatively assessed. The effect of the CSC symmetric division probability on the doubling time was also explored. The CSC symmetric division probability also affects the proportion of CSCs in the tumor and this relationship was investigated. Finally, doubling times and CSC proportions were compared with

1Department of Physics, University of Adelaide, North Terrace, Adelaide, South Australia, 5005, Australia. 2Department of Medical Physics, Royal Adelaide Hospital, North Terrace, Adelaide, South Australia, 5000, Australia. 3Sansom Institute for Health Research and the School of Health Sciences, University of South Australia, Adelaide, South Australia, Australia. Correspondence and requests for materials should be addressed to J.C.F. (email: Jake. Forster@adelaide.edu.au)
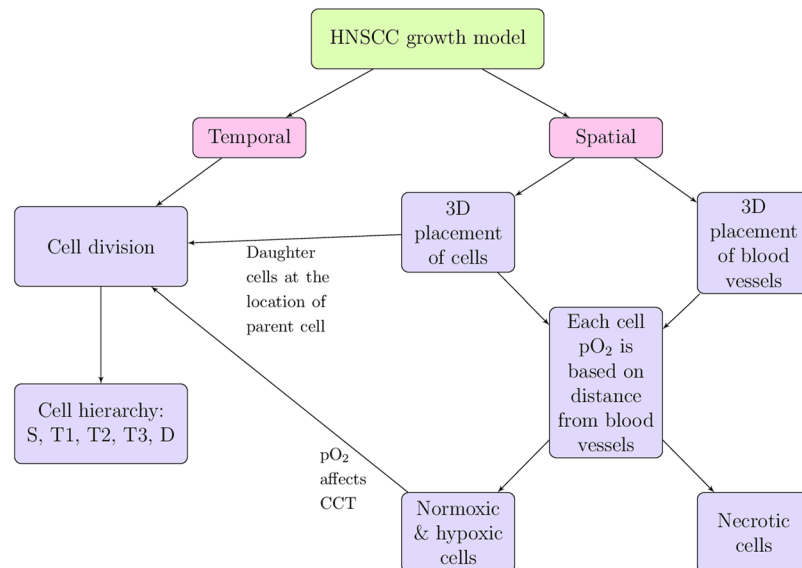
Figure 1. Main features of the HNSCC tumor growth model. Adapted with permission from ref. 10.

clinical data for HNSCC. While tumor irradiation was not simulated, tumor growth kinetics during accelerated repopulation were obtained by increasing the CSC symmetric division probability.

Methods

The tumor growth model.   Simulations of HNSCC tumor growth were performed using a computational model that was developed in-house using Matlab (version R2017a, The MathWorks, Inc.) and has been previously described[10]. The flow chart in Fig. 1 outlines the spatial and temporal features of the model and how they are related. Briefly, each tumor cell is modeled as an ellipsoid and packed into randomized positions in 3D space without overlap (Fig. 2a). The tumor grows over time by cell division, wherein a cell upon reaching the end of its cell cycle time (CCT) divides into two daughter cells, consequently pushing neighbouring cells outward towards the tumor periphery. A hierarchy of cell types is simulated, including CSCs, three generations of transit cells (T1-3) and differentiated cells (Fig. 2b). The probability for CSCs to undergo symmetric division (i.e., divide into two CSCs as opposed to one CSC and one transit cell) is set by the user. The sloughing of differentiated cells, which is characteristic of epithelial tissue, is also simulated.

Angiogenesis is modeled reflecting a connected and chaotic tumor vasculature that grows out with the cells (Fig. 2c,d), with blood vessels represented by consecutive discrete vessel units. Tumors can be grown with different vascularities which are quantified by the relative vascular volume, RVV. Cellular pO_2 is modeled dynamically as a function of distance from the nearest vessel using a diffusion equation (Table 1), with key parameters being the blood oxygenation, p_0, and the distance from vessels to the onset of necrosis (the necrosis distance, ND). The tumor vascularity (RVV) and the blood oxygenation (p_0 and ND) affect the amount of hypoxia in the tumor (Fig. 2e,f). Hypoxic cells have longer CCTs and cells that become necrotic are gradually resorbed by the tumor. Table 1 summarises the main parameters of the model and their values for HNSCC.

Simulations entail the following. First, a unique 3D mesh of non-overlapping cell/vessel unit positions is generated using Monte Carlo methods. The cell density reached is 2×10^8 cells/cm³. A connected network of blood vessels is then generated. As a result, a selection of the mesh positions are designated as vessel unit positions. A unique vasculature is generated each time using Monte Carlo methods. The vasculature is chaotic and tortuous, representative of tumor vasculature[1, 2]. As the tumor grows larger, the vasculature grows out by activating more of the vessel unit positions. Mesh positions that are not designated as vessel unit positions are cell positions, meaning tumor cells may occupy them during tumor growth simulation.

Once a blood vessel network has been generated and prior to tumor growth simulation, the oxygen tension at each cell position is determined and used to calculate the CCT. Cells push one another around when a cell divides, a differentiated cell is lost or a necrotic cell is resorbed. When a cell changes position, it retains its age (the time since it last divided), but its CCT changes to the CCT at its new position. When the age of the cell equals its position dependent CCT, it divides. When a cell divides, it pushes a neighbouring cell outward towards the tumor periphery, causing a chain of cell movement outward, making room for the additional daughter cell. Thus, one daughter cell occupies the position where the parent cell used to be, and the other daughter cell occupies an adjacent position.

The daughter cells are always one generation more differentiated than the parent cell (CSC → T1 → T2 → T3 → differentiated), except in the case of CSC symmetric division. A differentiated cell loss frequency of 80% is simulated to model the natural cell death of these cells, i.e., apoptosis. When a cell becomes differentiated, after a time equal to the CCT, there is an 80% likelihood that the differentiated cell is removed from the tumor. If it is not removed, it remains for another period of time equal to the CCT, then there is again an 80% likelihood that
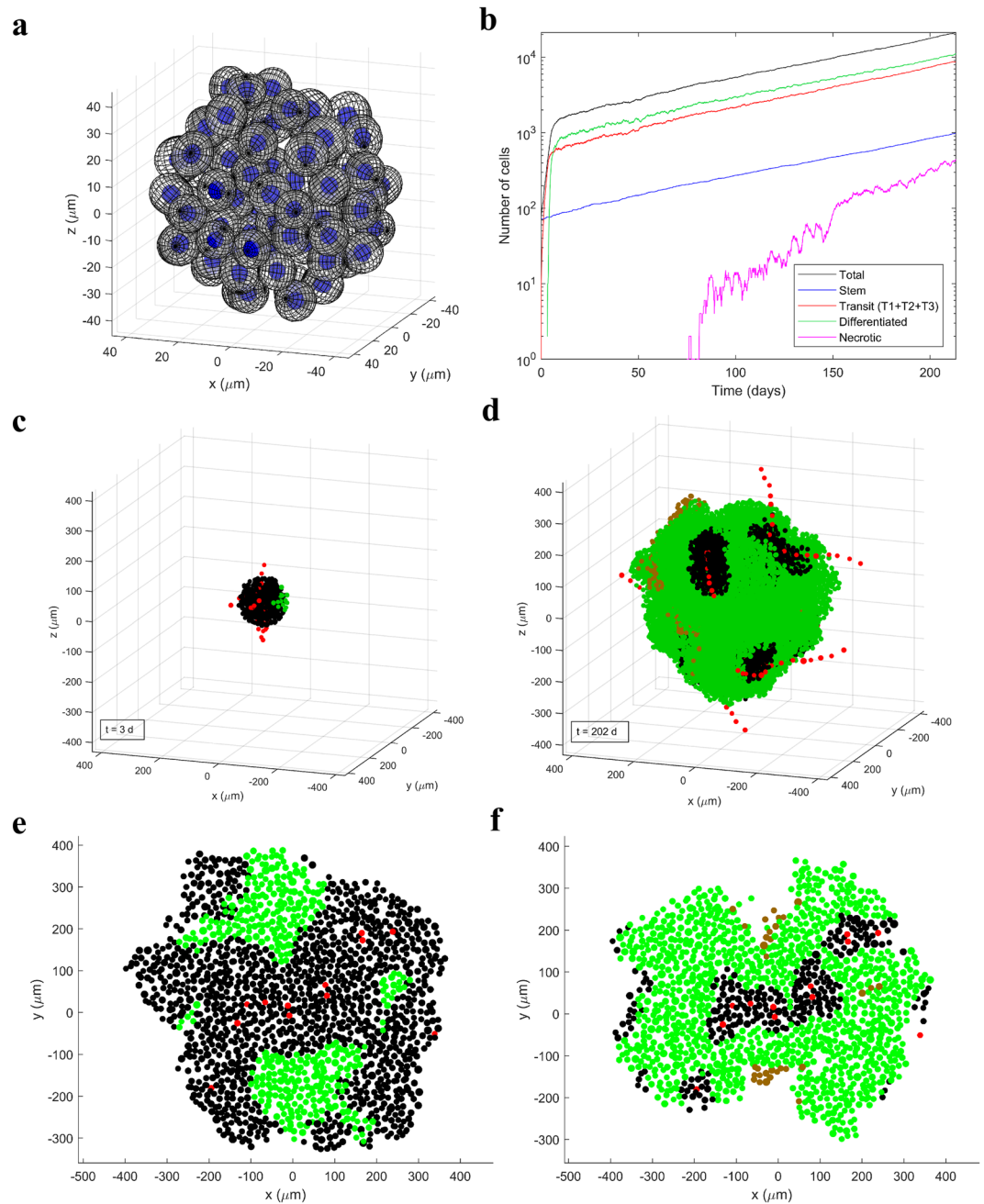
Figure 2. HNSCC tumor growth model. (**a**) Tumor cells are modeled as non-overlapping ellipsoids in randomized positions in 3D. (**b**) Cell kinetics for the different types of cells in an example simulation. (**c**,**d**) The tumor in the example simulation after 3 days and 202 days of growth. Vessel units are shown in red, normoxic cells in black, hypoxic cells ($pO_2 < 10$ mmHg) in green and necrotic cells in brown. Vessel units "string" together to form whole vessels that undergo branching in a chaotic fashion. Tumor cells close to vessels are normoxic, cells further from vessels are hypoxic and cells pushed further than ND from a vessel become necrotic. This example simulation started with approximately 70 CSCs and ended with $RVV = 0.4\%$, using $p_0 = 40$ mmHg, $ND = 180$ μm and CSC symmetric division probability $= 2\%$. (**e**,**f**) Sections of tumors with the same vasculature structure but different blood oxygenation (via p_0 and ND) ((**e**) $p_0 = 60$ mmHg and $ND = 220$ μm; (**f**) $p_0 = 30$ mmHg and $ND = 120$ μm). (**e**,**f**) were adapted with permission from ref. 10.

it is removed, and so on. When a differentiated cell is removed, there is a chain of cell movement inward to fill the vacant position. The same occurs when a necrotic cell is resorbed from the tumor, which occurs when its age reaches the necrotic cell resorption time (Table 1).

For a more in-depth description of the computational model methods, please refer to ref. 10.

Input parameter	Values	Type	References
Cell (and blood vessel) diameter	14–20 μm	Distribution	11, 36, 37
RVV	2–10%	Single value	11, 12
Oxygen tension	$p(r) = p_0 \frac{ND^2}{R_0^2}\left(2\ln\left(\frac{ND}{r}\right) - 1 + \frac{r^2}{ND^2}\right)$ where, $a = 10\,\mu m$	Distribution	38, 39
p_0	20–100 mmHg	Single value	11, 13
ND	80–300 μm	Single value	14, 15
CCT under normoxia	33 ± 5.9 h (Gaussian)	Distribution	40, 41
CCT adjustment factor with hypoxia	$y(pO_2) = 1 + 1.8e^{-0.2pO_2}$	Distribution	40, 42, 43
Hypoxia-induced quiescence	$pO_2 < 1$ mmHg	Single value	44–46
Necrotic cell resorption time	3–6 days depending on local necrotic volume	Distribution	47, 48
CSC symmetric division probability	~2% pre-treatment, possibly >50% during accelerated repopulation	Single value	6–8, 30, 40
Differentiated cell loss frequency	80%	Single value	40, 41

Table 1. Tumor growth model input parameters and values for HNSCC.

Study of tumor oxygenation.   The HNSCC tumor model was used in this work to quantify how the vascularity (RVV) and the blood oxygenation (p_0 and ND) affect the tumor oxygenation. Noting that HNSCC exhibit RVV from 2–10%[11, 12], p_0 from 20–100 mmHg[11, 13] and ND from 80–300 μm[14, 15], three combinations of (p_0, ND) were considered, namely (20 mmHg, 80 μm), (40 mmHg, 180 μm) and (100 mmHg, 300 μm), depicting scenarios of poor, moderate and high blood oxygenation, respectively. In each case, the model input parameter RVV_0 (which would be equal to the tumor RVV if the tumor grew with spherical symmetry, but due to preferential growth along the vessels, RVV ends up larger than RVV_0) was varied from 0–10% in 1% increments (for the (20 mmHg, 80 μm) combination, RVV_0 values of 0.25% and 0.5% were also used), yielding values of tumor RVV from 0–16%. The tumor RVV was determined at the end of the growth simulation as the ratio of the number of vessel units to the number of living cells + necrotic cells + vessel units (×100%). Tumor growth simulations began with approximately 70 CSCs and ended with a final tumor diameter of 1 mm (10^4–10^5 cells). A CSC symmetric division probability of 50% was used in the tumor oxygenation study for fast computations, since this affects the doubling time and CSC proportion but does not greatly affect the tumor oxygenation.

The tumor oxygenation at the end of the growth simulation was evaluated using several different descriptors. The hypoxic proportions HP_{10}, HP_5, $HP_{2.5}$ and HP_1 were determined, which were the proportions of living cells with $pO_2 <$ 10, 5, 2.5 and 1 mmHg, respectively. The mean and median cellular pO_2 in living cells were also calculated. The volume proportion of necrosis (necrotic volume) was evaluated as the ratio of the number of necrotic cells to the number of living cells + necrotic cells + vessel units (×100%).

Study of tumor growth rate and CSC proportion.   The HNSCC tumor model was then used to explore the effects of tumor oxygenation and CSC symmetric division on the doubling time and the CSC proportion. The doubling time, T_d, in the final days (in "tumor time") of the tumor growth simulation was evaluated as follows. Let $N(t)$ denote the number of living and necrotic cells in the tumor at time t. Then the average slope, k, of the curve $\ln N$ vs t in the final few days of the simulation was used to calculate the final doubling time according to:

$$T_d = \ln 2/k$$

The effect of tumor hypoxia and necrosis on doubling time was observed in the simulations from the tumor oxygenation study. Since these simulations all used a CSC symmetric division probability of 50%, the relative variation in the doubling time was reported.

To investigate the effects of the CSC symmetric division probability on the doubling time and the CSC proportion, CSC symmetric division probabilities of 2%, 5%, 10%, 25%, 50%, 75% and 100% were simulated for the two extremes of HNSCC tumor oxygenation. The most oxygenated case was RVV = 10%, $p_0 = 100$ mmHg and ND = 300 μm and the most hypoxic case was RVV = 2%, $p_0 = 20$ mmHg and ND = 80 μm. In order to achieve approximately these RVVs, the model parameter RVV_0 was set to 8.2% and 0.75% respectively. Again, the simulations began with approximately 70 CSCs and ended with a final tumor diameter of 1 mm. Three simulations (n = 3) were conducted for each value of CSC symmetric division probability for both well oxygenated and severely hypoxic cases (with the exception of the severely hypoxic case with CSC symmetric division probability 10%, for which n = 4 was used). The CSC proportion was calculated as the ratio of the number of CSCs to the number of living cells (×100%). The doubling times and CSC proportions were plotted using the mean value of the 3 (or 4) simulation runs and with error bars corresponding to the standard error of the mean (SEM). Prism (version 7, GraphPad Software, Inc.) was used to determine whether statistical significance had been reached.

Equipment.   Simulations were performed on the Phoenix cluster at the University of Adelaide[16] using as many as 12 cores and 10 GB of RAM.

Data availability.   The data that support the finding of this study are available from the corresponding author upon reasonable request.
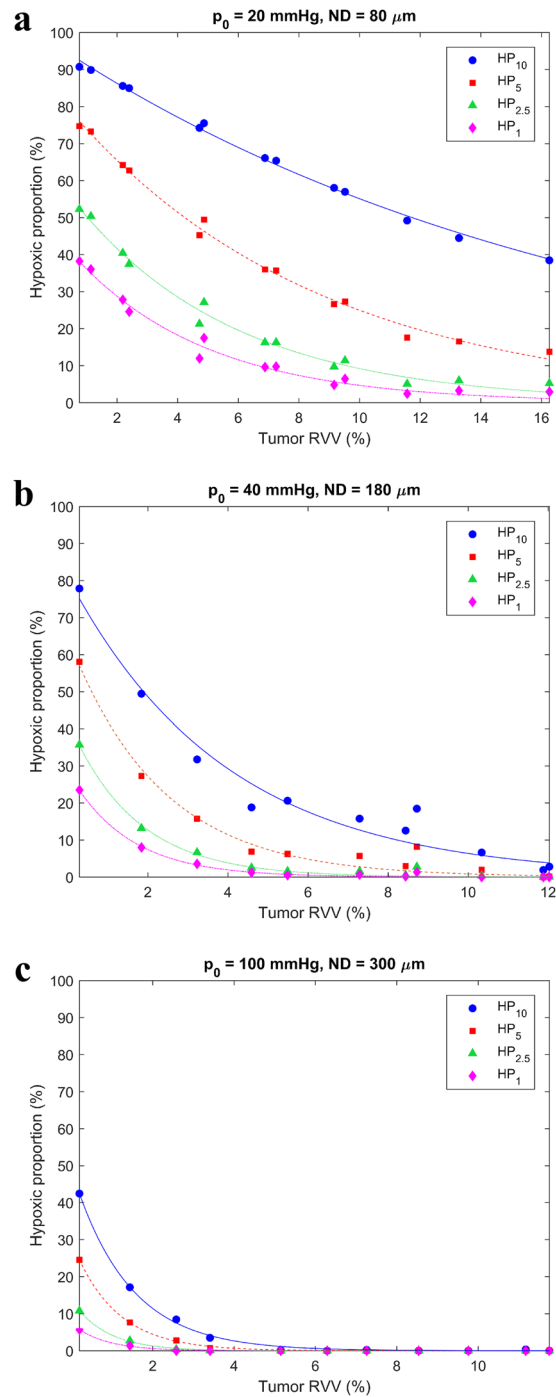
Figure 3. Variation of hypoxic proportions with tumor vascularity for (**a**) poor blood oxygenation ($p_0 = 20$ mmHg and $ND = 80$ µm), (**b**) moderate blood oxygenation ($p_0 = 40$ mmHg and $ND = 180$ µm) and (**c**) high blood oxygenation ($p_0 = 100$ mmHg and $ND = 300$ µm).

Code availability. The code used to analyze the data is available from the corresponding author upon reasonable request. The code used to perform tumor growth simulations has not been made publicly available at this time.

Results

The effects of tumor vascularity and blood oxygenation on tumor oxygenation. With increasing tumor vascularity (*RVV*) and increasing blood oxygenation (p_0 and *ND*), the hypoxic proportions and necrotic volume decreased, while the mean and median cellular pO$_2$ increased (Figs 3 and 4). According to clinical data, HNSCC exhibit *RVV* from 2–10%[11, 12], p_0 from 20–100 mmHg[11, 13] and *ND* from 80–300 µm[14, 15]. With these constraints, the tumor growth model predicted values of HP$_1$ from 0–29%, HP$_{2.5}$ from 0–42%, HP$_5$ from 0–65%, HP$_{10}$
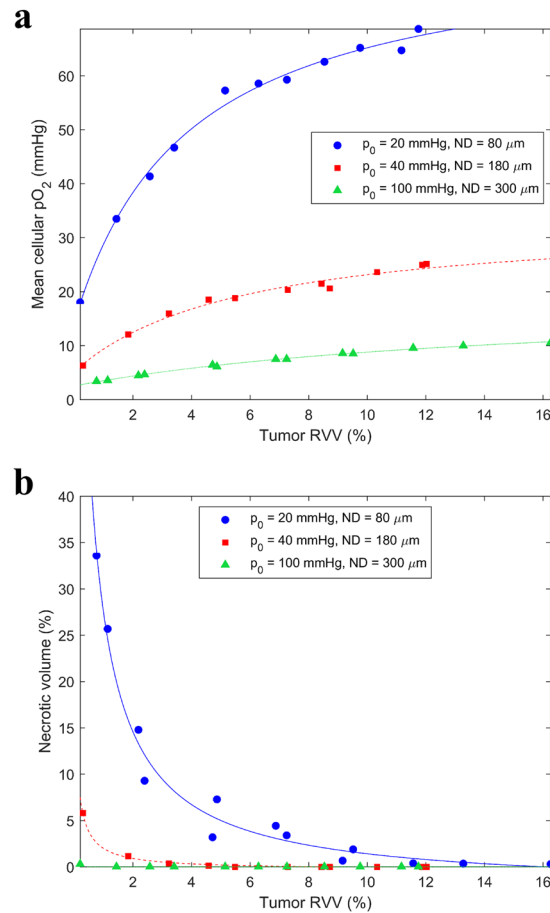
Figure 4. Variation of (**a**) mean cellular pO$_2$ and (**b**) necrotic volume with tumor vascularity for poor, moderate and high blood oxygenation.

from 0–86%, mean cellular pO$_2$ from 4.4–65.2 mmHg, median cellular pO$_2$ from 2.9–67.5 mmHg and necrotic volume from 0–15% for HNSCC.

For poor blood oxygenation ($p_0 = 20$ mmHg and $ND = 80$ μm), there was necrosis present even at 10% *RVV*. Note that the same hypoxic proportion could arise from different combinations of *RVV*, p_0 and *ND*. For example, (*RVV*, p_0, *ND*) combinations of (11.8%, 20 mmHg, 80 μm), (2.7%, 40 mmHg, 180 μm) and (0.4%, 100 mmHg, 300 μm) each yielded a HP$_5$ of 20%.

The effects of hypoxia and CSC symmetric division on the tumor growth rate and the CSC proportion. The doubling time decreased with increasing tumor vascularity (*RVV*) and increasing blood oxygenation (p_0 and *ND*) (Fig. 5a). For HNSCC (*RVV* = 2–10%, $p_0 = 20$–100 mmHg, *ND* = 80–300 μm), the doubling time increased by a factor of 3 from well oxygenated tumors to the most hypoxic tumors. The doubling time was considerably affected, even without the presence of necrosis, by low cellular pO$_2$ effects such as increased CCTs and cell quiescence (Fig. 5b,c).

The doubling time decreased with increasing probability of CSC symmetric division probability (Fig. 6a). The mean doubling time was 2.6–3.3 times larger for the most hypoxic tumors than for well oxygenated tumors of HNSCC across all values of CSC symmetric division probability. The difference in doubling time between severely hypoxic and well oxygenated conditions was significant (p-value < 0.05 using unpaired t-test with Welch's correction) at every value of CSC symmetric division probability.

The CSC proportion increased with CSC symmetric division probability (Fig. 6b). The mean CSC proportion was 1–1.14 times larger for the most hypoxic tumors than for well oxygenated tumors across all values of CSC symmetric division probability. The difference in CSC proportion between severely hypoxic and well oxygenated conditions was significant (p-value <0.05 using unpaired t-test with Welch's correction) at every value of CSC symmetric division probability except 2%.

A CSC symmetric division probability of 2% yielded a mean ± SEM doubling time of 44.5 ± 0.8 days (n = 3) for well oxygenated tumors and 129 ± 16 days (n = 3) for the most hypoxic tumors. The CSC proportion was approximately 6% in each case (6.11 ± 0.01% (n = 3) and 6.3 ± 0.2% (n = 3) respectively). An increase in the CSC symmetric division probability to 50% yielded a doubling time of 2.28 ± 0.03 days (n = 3) for well oxygenated tumors and 6.3 ± 0.6 days (n = 3) for the most hypoxic tumors. The CSC proportions were 30.49 ± 0.06% (n = 3) and 34.8 ± 0.3% (n = 3) respectively.

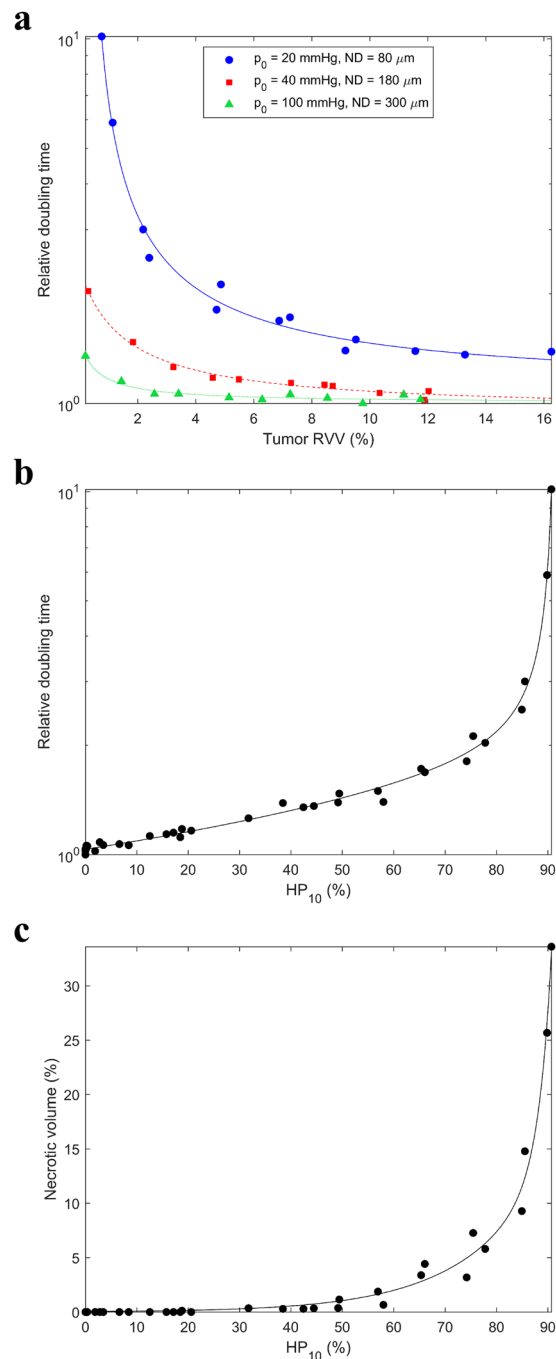**Figure 5.** Relative variation in the doubling time with (**a**) tumor vascularity and (**b**) HP_{10}. (**c**) Variation in the necrotic volume with HP_{10}.

Discussion

Several studies have reported pO_2 measurements in human HNSCC using invasive polarographic needle electrodes. The results from some of these studies are collated in Table 2. Since accessing a tissue block from the HNSCC primary tumor can be difficult, these studies often took measurements from sufficiently large lymph node metastases originating from a primary HNSCC. The table also lists measurements of necrotic volume in HNSCCs, as assessed by CT scan or MRI. The results from the current study are included at the bottom for comparison.

The values of median pO_2, mean pO_2, $HP_{2.5}$, HP_5 and HP_{10} produced by the tumor growth model using RVV from 2–10%, p_0 from 20–100 mmHg and ND from 80–300 μm are in line with these clinical measurements. This assists in model validation since these values for RVV, p_0 and ND are based on clinical data for HNSCC. The clinical tumor oxygenation data overall indicate well oxygenated tumors are rare and lower values of RVV, p_0 and ND are typical.
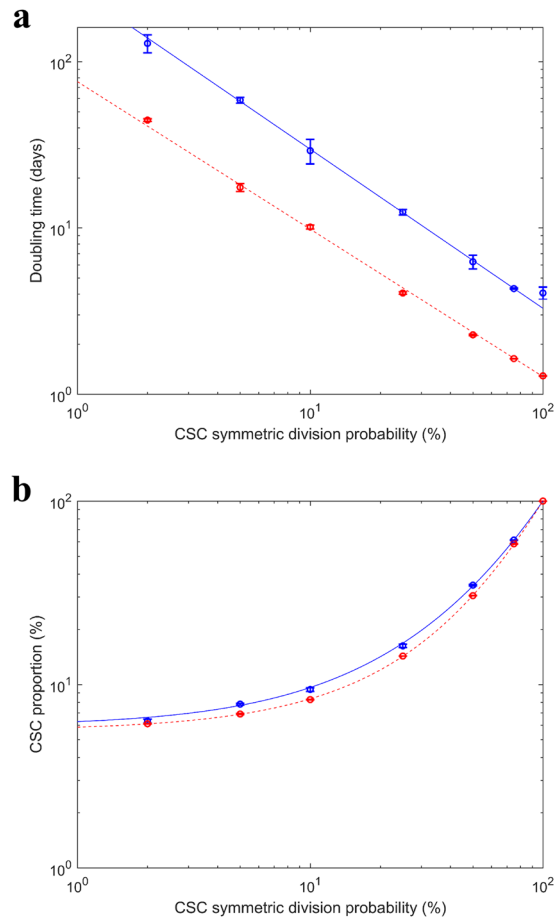
Figure 6. Variation of (**a**) doubling time and (**b**) CSC proportion with CSC symmetric division probability for severely hypoxic tumors (mean $\pm$ SD $RVV = 2.2 \pm 0.2\%$ (n $=$ 22), $p_0 = 20$ mmHg, $ND = 80\,\mu$m) (blue) and well oxygenated tumors (mean $\pm$ SD $RVV = 10.5 \pm 0.6\%$ (n $=$ 21), $p_0 = 100$ mmHg, $ND = 300\,\mu$m) (red) of HNSCC.

The clinical studies sometimes reported large values of necrotic volume outside the range produced by the tumor growth model. This is likely because the clinical studies observed macroscopic regions of necrosis. Macroscopic necrosis occurs when tumors become large and whole macroscopic regions of the tumor lose blood supply. The tumor growth model only produced necrosis at the microscopic scale (between distant blood vessels) in the sub-clinical sized tumors used in this study.

Pre-treatment doubling times of HNSCC have been obtained in studies that measured tumor growth while patients waited for treatment. Jensen et al.[17] found that in the time between diagnostic scan (MR or CT) and treatment planning CT scan (median 28 days, range 5–95 days), the median doubling time was 99 days (range 15 to > 234 days) for 61 patients with HNSCC. Waaijer et al.[18] found that in the time between diagnostic and treatment planning CT scans (mean 34 days), the mean doubling time was 96 days (range 21–256 days) in 13 patients with oropharyngeal SCC. Murphy et al.[19] found that in the time between diagnostic (MRI or CT) and planning or interval CT scan (median 35 days, range 8–314 days), the median doubling time was 94 days (range 16–6931 days) in 85 oropharyngeal SCC. These average clinically measured pre-treatment doubling times are similar to those produced by the presented tumor growth model under moderately hypoxic conditions and with a CSC symmetric division probability of approximately 2% (recall the doubling times obtained with the tumor model using 2% CSC symmetric division averaged 45 days for well oxygenated tumors and 130 days for severely hypoxic tumors).

In the current work, a CSC symmetric division probability of 2% yielded a proportion of CSCs in the tumor of approximately 6% for all HNSCC tumor oxygenation levels. Methods have been established for identifying CSCs in HNSCC. For example, cells that express markers such as ALDH1, CD133 and CD44 exhibit CSC-like properties, while others do not[9, 20–24]. Cells that efficiently efflux Hoechst 33342 dye, termed side-population (SP) cells, are also CSC-like[25, 26]. Chinn et al.[27] reported a mean CD44^{high} content of 10.8% (range 0–84.5%) for 40 patient-derived primary HNSCCs. In 10 human oral SCC tissue samples, Zhang et al.[28] found CD133^{+} content of 1–3%. Lu et al.[29] identified approximately 2.1% SP cells in 7 human primary HNSCC samples, and all SP cells were also CD133^{+}. The CSC proportion of 6% obtained by the tumor growth model using 2% CSC symmetric division, is close to these clinical estimates for HNSCC pre-treatment and results from other models (e.g. 5.9% from Marcu & Marcu[30]).

	Tumor site	Median pO$_2$ (mmHg) in the tumor	Mean pO$_2$ (mmHg) in the tumor	HP$_{2.5}$ (%)	HP$_5$ (%)	HP$_{10}$ (%)	Necrotic volume (%)
King et al.[49]	Metastastic cervical nodes from HNSCC	—	—	—	—	—	mean ± SD 19.09 ± 13.94 (n = 106)
Kong et al.[50]	Primary HNSCC	mean 14.0 (n = 82)	—	—	—	—	—
Gagel et al.[51]	lymph node metastases from HNSCC	mean ± SD 12.5 ± 10.3; range 0.1–41.1 (n = 38)	mean ± SD 17.6 ± 7.3; range 8.8–36.0 (n = 38)	mean ± SD 29.3 ± 18.4; range 0.0–58.5 (n = 38)	mean ± SD 38.4 ± 18.1; range 7.0–73.6 (n = 38)	mean ± SD 48.9 ± 18.2; range 13.0–78.7 (n = 38)	—
Nordsmark et al.[3]	Neck node metastases from HNSCC or primary HNSCC	median 9; range 0–62 (n = 397)		median 19; range 0–97 (n = 397)	median 38; range 0–100 (n = 397)	—	—
Kuhnt et al.[52]	Primary HNSCC	—	—	—	—	—	mean ± SD 18 ± 30 (n = 51)*
Gagel et al.[53]	neck lymph node metastases from HNSCC	mean 10.7; 95% CI of mean 5.2–16.1; range 0.4–22.4 (n = 16)	mean 16.3; 95% CI of mean 12.1–20.5; range 9.0–27.4 (n = 16)	mean 35.9; 95% CI of mean 24.1–47.6; range 0.5–58.1 (n = 16)	mean 44.3; 95% CI of mean 34.0–54.5; range 27.6–66.5 (n = 16)	mean 52.5; 95% CI of mean 42.2–62.9; range 33.7–77.5 (n = 16)	—
Terris et al.[54]	cervical lymph node metastases from HNSCC	—	mean ± SD 20.8 ± 13.7 (n = 50)*	mean ± SD 20.8 ± 25.7 (n = 42)	—	—	mean ± SD 14.5 ± 11.2 (n = 42)
Brizel et al.[55]	Primary HNSCC or cervical lymph node from HNSCC	mean 4.5; range 0–60 (n = 63)*	—	—	—	—	—
Brizel et al.[5]	Primary HNSCC or neck node metastases from HNSCC	mean 11.2; range 0.4–60 (n = 28)	—	—	—	—	—
Nordsmark et al.[4]	Lymph node metastases from HNSCC (n = 34) or primary HNSCC (n = 1)	mean ± SD 14.7 ± 10.8; median 14; range 1–35 (n = 35)		mean ± SD 22 ± 24; median 15; range 0–95 (n = 35)	mean ± SD 35 ± 29; median 29; range 0–100 (n = 35)	—	—
The current work		range 2.9–67.5	range 4.4–65.2	range 0–42	range 0–65	range 0–86	range 0–15

Table 2. Clinical data for tissue pO$_2$ and necrotic volume in human HNSCC. *Mean ± SD of two or more subgroups were combined with appropriate error propagation.

Tumors respond to treatment by undergoing accelerated repopulation. In an analysis of 5 clinical trials containing a total of 2653 patients, Pedicini et al.[31] using an analytical/graphical method arrived at a best estimate of 3.5 days (95% CI 3.1–3.9 days) for the doubling time of HNSCC during radiotherapy. The loss of asymmetric division by CSCs is believed to be a key mechanism behind accelerated repopulation[6–8, 30, 32, 33]. In the tumor growth model, a CSC symmetric division probability of 50% yielded doubling times from 2.3 to 6.1 days, depending on the tumor oxygenation, which are in line with the estimate by Pedicini et al. A 50% CSC symmetric division probability yielded CSC proportions from 30–35% in the current work. To the authors' knowledge, there are no clinical studies in the literature that measured the CSC proportion in HNSCC in patients during accelerated repopulation. In the model by Marcu & Marcu[30], the CSC proportions obtained were higher than in the current work for the same CSC symmetric division probability. For example, in their work, 10%, 20% and 30% symmetric division yielded 25%, 35% and 45% CSCs, respectively (recall in the current work, 10% and 25% symmetric division yielded approximately 9% and 15% CSCs, respectively). Conversely, the CSC proportions were slightly lower in the HYP-RT model by Harriss-Phillips et al.[33] than in the current work. In that model, 30% symmetric division yielded just 10% CSCs. Most in vitro studies of various cancer types show a 3–5 times increase in CSCs post single irradiation[24].

Conclusion

The current work established how the tumor oxygenation varies with vascularity and blood oxygenation, how the doubling time varies with tumor oxygenation and CSC symmetric division probability, and how the CSC proportion varies with CSC symmetric division probability in a 4D cellular model of HNSCC tumor growth. The doubling time varied by a factor of ~3 from well oxygenated tumors to the most severely hypoxic tumors of HNSCC. A CSC symmetric division probability of 2% yielded clinically relevant doubling times and CSC proportions for HNSCC before treatment, while a value of 50% produced the doubling times observed in the clinic for HNSCC undergoing accelerated repopulation. This 50% probability yielded CSC proportions from 30–35%.

In future work, the tumor growth model will be extended to a radiotherapy simulation tool for both low and high LET beams. The cellular geometry will be imported into Geant4[34] and irradiated in Monte Carlo track structure simulations. Radiolysis will be simulated along the particle tracks. Ionisation events and generated •OH species will be clustered in the cell nuclei to predict the complexity and extent of DNA damage to each cell. The cellular pO$_2$ will affect how efficiently •OH attack to the base of DNA is translated to strand breakage[35]. Irradiation will be simulated in fractions separated by time intervals, during which the tumor growth model will translate DNA damage to cell death while also regrowing the tumor.

References

1. Carmeliet, P. & Jain, R. K. Angiogenesis in cancer and other diseases. *Nature* **407**, 249–257 (2000).
2. Forster, J. C., Harriss-Phillips, W. M., Douglass, M. J. & Bezak, E. A review of the development of tumor vasculature and its effects on the tumor microenvironment. *Hypoxia (Auckl)* **5**, 21–32 (2017).
3. Nordsmark, M. *et al.* Prognostic value of tumor oxygenation in 397 head and neck tumors after primary radiation therapy. An international multi-center study. *Radiother. Oncol.* **77**, 18–24 (2005).
4. Nordsmark, M., Overgaard, M. & Overgaard, J. Pretreatment oxygenation predicts radiation response in advanced squamous cell carcinoma of the head and neck. *Radiother. Oncol.* **41**, 31–39 (1996).
5. Brizel, D. M., Sibley, G. S., Prosnitz, L. R., Scher, R. L. & Dewhirst, M. W. Tumor hypoxia adversely affects the prognosis of carcinoma of the head and neck. *Int. J. Radiat. Oncol. Biol. Phys.* **38**, 285–289 (1997).
6. Dörr, W. Three A's of repopulation during fractionated irradiation of squamous epithelia: Asymmetry loss, Acceleration of stem-cell divisions and Abortive divisions. *Int. J. Radiat. Biol.* **72**, 635–643 (1997).
7. Trott, K. R. & Kummermehr, J. Rapid repopulation in radiotherapy: a debate on mechanism. Accelerated repopulation in tumours and normal tissues. *Radiother. Oncol.* **22**, 159–160 (1991).
8. Withers, H. R. & Elkind, M. M. Radiosensitivity and fractionation response of crypt cells of mouse jejunum. *Radiat. Res.* **38**, 598–613 (1969).
9. Krishnamurthy, S. & Nör, J. E. Head and neck cancer stem cells. *J. Dent. Res.* **91**, 334–340 (2012).
10. Forster, J. C., Douglass, M. J., Harriss-Phillips, W. M. & Bezak, E. Development of an in silico stochastic 4D model of tumor growth with angiogenesis. *Med. Phys.* **44**, 1563–1576 (2017).
11. Amelink, A. *et al.* Non-invasive measurement of the morphology and physiology of oral mucosa by use of optical spectroscopy. *Oral Oncol.* **44**, 65–71 (2008).
12. Pazouki, S. *et al.* The association between tumour progression and vascularity in the oral mucosa. *J. Pathol.* **183**, 39–43 (1997).
13. Carreau, A., El Hafny-Rahbi, B., Matejuk, A., Grillon, C. & Kieda, C. Why is the partial oxygen pressure of human tissues a crucial parameter? Small molecules and hypoxia. *J. Cell. Mol. Med.* **15**, 1239–1253 (2011).
14. Beasley, N. J. *et al.* Carbonic anhydrase IX, an endogenous hypoxia marker, expression in head and neck squamous cell carcinoma and its relationship to hypoxia, necrosis, and microvessel density. *Cancer Res.* **61**, 5262–5267 (2001).
15. Wijffels, K. I. *et al.* Vascular architecture and hypoxic profiles in human head and neck squamous cell carcinomas. *Br. J. Cancer* **83**, 674–683 (2000).
16. Phoenix High Performance Computing. *University of Adelaide* https://www.adelaide.edu.au/phoenix/ (2017)
17. Jensen, A. R., Nellemann, H. M. & Overgaard, J. Tumor progression in waiting time for radiotherapy in head and neck cancer. *Radiother. Oncol.* **84**, 5–10, doi:10.1016/j.radonc.2007.04.001 (2007).
18. Waaijer, A. *et al.* Waiting times for radiotherapy: consequences of volume increase for the TCP in oropharyngeal carcinoma. *Radiother. Oncol.* **66**, 271–276 (2003).
19. Murphy, C. T. *et al.* Pre-treatment tumor-specific growth rate as a temporal biomarker that predicts treatment failure and improves risk stratification for oropharyngeal cancer. *Oral Oncol.* **51**, 1034–1040 (2015).
20. Islam, F., Gopalan, V., Wahab, R., Smith, R. A. & Lam, A. K. Cancer stem cells in oesophageal squamous cell carcinoma: Identification, prognostic and treatment perspectives. *Crit. Rev. Oncol. Hematol.* **96**, 9–19 (2015).
21. Zhang, Z., Filho, M. S. & Nör, J. E. The biology of head and neck cancer stem cells. *Oral Oncol.* **48**, 1–9 (2012).
22. Albers, A. E. *et al.* Stem cells in squamous head and neck cancer. *Crit. Rev. Oncol. Hematol.* **81**, 224–240 (2012).
23. Prince, M. E. & Ailles, L. E. Cancer stem cells in head and neck squamous cell cancer. *J. Clin. Oncol.* **26**, 2871–2875 (2008).
24. Reid, P., Wilson, P., Li, Y., Marcu, L. G. & Bezak, E. Current Understanding of Cancer Stem Cells: Review of their Radiobiology and role in Head and Neck Cancers. *Head Neck* (2017).
25. Tabor, M. H. *et al.* Head and neck cancer stem cells: the side population. *Laryngoscope* **121**, 527–533 (2011).
26. Sun, G. *et al.* Identification of stem-like cells in head and neck cancer cell lines. *Anticancer Res.* **30**, 2005–2010 (2010).
27. Chinn, S. B. *et al.* Cancer stem cells: mediators of tumorigenesis and metastasis in head and neck squamous cell carcinoma. *Head Neck* **37**, 317–326 (2015).
28. Zhang, Q. *et al.* A subpopulation of CD133(+) cancer stem-like cells characterized in human oral squamous cell carcinoma confer resistance to chemotherapy. *Cancer Lett.* **289**, 151–160 (2010).
29. Lu, B. C. *et al.* Elevated expression of Nrf2 mediates multidrug resistance in CD133 + head and neck squamous cell carcinoma stem cells. *Oncol. Lett.* **12**, 4333–4338 (2016).
30. Marcu, L. G. & Marcu, D. In silico modelling of a cancer stem cell-targeting agent and its effects on tumour control during radiotherapy. *Sci. Rep.* **30**, 32332 (2016).
31. Pedicini, P., Caivano, R., Fiorentino, A. & Strigari, L. Clinical radiobiology of head and neck cancer: the hypothesis of stem cell activation. *Clin. Transl. Oncol.* **17**, 469–476 (2015).
32. Harriss-Phillips, W. M., Bezak, E. & Yeoh, E. K. Monte Carlo radiotherapy simulations of accelerated repopulation and reoxygenation for hypoxic head and neck cancer. *Br. J. Radiol.* **84**, 903–918 (2011).
33. Harriss-Phillips, W. M., Bezak, E. & Yeoh, E. The HYP-RT Hypoxic Tumour Radiotherapy Algorithm and Accelerated Repopulation Dose per Fraction Study. *Comput. Math. Methods Med.* **2012**, 363564 (2012).
34. Allison, J. *et al.* Recent developments in GEANT4. *Nucl. Instrum. Methods Phys. Res. A* **835**, 186–225 (2016).
35. Wardman, P. The importance of radiation chemistry to radiation and free radical biology (The 2008 Silvanus Thompson Memorial Lecture). *Br. J. Radiol.* **82**, 89–104 (2009).
36. Vlad, R. M., Alajez, N. M., Giles, A., Kolios, M. C. & Czarnota, G. J. Quantitative ultrasound characterization of cancer radiotherapy effects *in vitro*. *Int. J. Radiat. Oncol. Biol. Phys.* **72**, 1236–1243 (2008).
37. Amelink, A., Sterenborg, H. J., Bard, M. P. & Burgers, S. A. *In vivo* measurement of the local optical properties of tissue by use of differential path-length spectroscopy. *Opt. Lett.* **29**, 1087–1089 (2004).
38. Tannock, I. F. Oxygen diffusion and the distribution of cellular radiosensitivity in tumours. *Br. J. Radiol.* **45**, 515–524 (1972).
39. Carlson, D. J., Keall, P. J., Loo, B. W. Jr., Chen, Z. J. & Brown, J. M. Hypofractionation results in reduced tumor cell kill compared to conventional fractionation for tumors with regions of hypoxia. *Int. J. Radiat. Oncol. Biol. Phys.* **79**, 1188–1195 (2011).
40. Harriss, W. M. Monte Carlo Modelling of Tumour Growth, Hypoxia and Radiotherapy in Head and Neck Squamous Cell Carcinoma (PhD Thesis). University of Adelaide, Adelaide (2011).
41. Marcu, L. G. Tumour repopulation and the role of abortive division in squamous cell carcinomas during chemotherapy. *Cell Prolif.* **47**, 318–325 (2014).
42. Hirst, D. G. & Denekamp, J. Tumour cell proliferation in relation to the vasculature. *Cell Tissue Kinet.* **12**, 31–42 (1979).
43. Alarcón, T., Byrne, H. M. & Maini, P. K. A mathematical model of the effects of hypoxia on the cell-cycle of normal and cancer cells. *J. Theor. Biol.* **229**, 395–411 (2004).
44. Amellem, O. & Pettersen, E. O. Cell inactivation and cell cycle inhibition as induced by extreme hypoxia: the possible role of cell cycle arrest as a protection against hypoxia-induced lethal damage. *Cell Prolif.* **24**, 127–141 (1991).
45. Douglas, R. M. *et al.* Hypoxia induces major effects on cell cycle kinetics and protein expression in Drosophila melanogaster embryos. *Am. J. Physiol. Regul. Integr. Comp. Physiol.* **288**, R511–R521 (2005).
46. Royds, J. A., Dower, S. K., Qwarnstrom, E. E. & Lewis, C. E. Response of tumour cells to hypoxia: role of p53 and NFκB. *Mol. Pathol.* **51**, 55–61 (1998).

47. Borkenstein, K., Levegrün, S. & Peschke, P. Modeling and computer simulations of tumor growth and tumor response to radiotherapy. *Radiat. Res.* **162**, 71–83 (2004).
48. Harting, C., Peschke, P., Borkenstein, K. & Karger, C. P. Single-cell-based computer simulation of the oxygen-dependent tumour response to irradiation. *Phys. Med. Biol.* **52**, 4775–4789 (2007).
49. King, A. D. *et al.* Cervical nodal metastases from head and neck squamous cell carcinoma: MRI criteria for treatment assessment. *Head Neck* **38**, E1598–E1604 (2016).
50. Kong, C. S. *et al.* The relationship between human papillomavirus status and other molecular prognostic markers in head and neck squamous cell carcinomas. *Int. J. Radiat. Oncol. Biol. Phys.* **74**, 553–561 (2009).
51. Gagel, B. *et al.* pO polarography, contrast enhanced color duplex sonography (CDS), [18F] fluoromisonidazole and [18F] fluorodeoxyglucose positron emission tomography. *BMC Cancer* **7**, 113 (2007).
52. Kuhnt, T. *et al.* Impact of tumor control and presence of visible necrosis in head and neck cancer patients treated with radiotherapy or radiochemotherapy. *J. Cancer Res. Clin. Oncol.* **131**, 758–764 (2005).
53. Gagel, B. *et al.* pO(2) Polarography versus positron emission tomography ([(18)F] fluoromisonidazole, [(18)F]-2-fluoro-2′-deoxyglucose). *An appraisal of radiotherapeutically relevant hypoxia. Strahlenther. Onkol.* **180**, 616–622 (2004).
54. Terris, D. J. Head and neck cancer: the importance of oxygen. *Laryngoscope* **110**, 697–707 (2000).
55. Brizel, D. M., Dodge, R. K., Clough, R. W. & Dewhirst, M. W. Oxygenation of head and neck cancer: changes during radiotherapy and impact on treatment outcome. *Radiother. Oncol.* **53**, 113–117 (1999).

Author Contributions

J.F. conceptualized and developed the model under the supervision of M.D., W.H. and E.B., based on their previous work and the idea of a 4D spatial-temporal tumor model. All authors were involved in manuscript preparation. While J.F. wrote the bulk of the manuscript, M.D., W.H. and E.B. provided input, feedback and revisions.

Additional Information

Publisher's note: Springer Nature remains neutral with regard to jurisdictional claims in published maps and institutional affiliations.